Scientific paper

# Fibrous Silica KCC-1 as a Platform for Mn-Based Dual Metal Oxide Adsorbents for CO<sub>2</sub> Capture

## Syawal Mohd Yusof,<sup>1,2</sup> Azizul Hakim Lahuri,<sup>1,\*</sup> Nurul Asikin Mijan,<sup>2</sup> Umar Kalmar Nizar,<sup>3</sup> Siti Sarahah Sulhadi,<sup>1</sup> Salma Samidin,<sup>2</sup> Ainil Hafiza Abdul Aziz<sup>1</sup>

<sup>1</sup> Department of Science and Technology, Universiti Putra Malaysia Sarawak, Nyabau Road, P.O. Box 396, 97008 Bintulu, Sarawak, Malaysia.

<sup>2</sup> Department of Chemical Science, Faculty of Science and Technology, Universiti Kebangsaan Malaysia, 43600, Bangi, Selangor, Malaysia.

<sup>3</sup> Chemistry Department, Faculty of Mathematic and Natural Science, Universitas Negeri Padang.

\* Corresponding author: E-mail: azizulhakim@upm.edu.my

Received: 06-19-2025

### **Abstract**

The continuous rise in atmospheric CO<sub>2</sub> levels due to industrial emissions and fossil fuel combustion has intensified the need for efficient carbon capture. Solid adsorbents are favoured for their reusability and low energy demand, yet often face limitations in thermal stability and adsorption performance. This study examines the effect of co-loading manganese (Mn) with potassium (K), copper (Cu), and calcium (Ca) on fibrous silica KCC-1 for CO<sub>2</sub> capture over a wide temperature range. KCC-1 was synthesised via a microemulsion method, and metals were introduced using an ultrasonic-surfactant-assisted impregnation technique. Characterisation using XRD, FTIR, BET, FESEM-EDX, and CO<sub>2</sub>-TPD confirmed structural integrity, surface functionality, and adsorption behaviour. CaO-MnO@KCC-1 shows the most balanced textural properties and the highest CO<sub>2</sub> uptake due to its strong basicity and varied adsorption site strength. This highlights its potential as a temperature-flexible CO<sub>2</sub> adsorbent.

 $\textbf{Keywords:} \ CO_2 \ capture; \ Manganese-based \ catalysts; Fibrous \ silica \ KCC-1; \ Ultrasonic-Surfactant-assisted \ impregnation; \\ metal \ dispersion; \ Basicity \ and \ redox \ properties$ 

### 1. Introduction

The continuous rise in atmospheric CO<sub>2</sub> concentration due to industrial processes and the burning of fossil fuels has intensified global warming and climate change.<sup>1</sup> CO<sub>2</sub> capture and storage (CCS) technology have therefore become essential for addressing these environmental issues. Solid sorbents have drawn the most attention among the several CCS techniques because of its efficiency, reusability, and potential for large-scale applications.<sup>2–5</sup>

The search for "smart sorbents" that can effectively absorb  $\mathrm{CO}_2$  at a variety of temperatures is still an intriguing area of materials science, nevertheless. Despite the progress made in CCS development, challenges remain in designing adsorbents capable of performing efficiently at different operational temperatures. The adsorption perfor-

mance of a material is primarily influenced by the strength and nature of the interaction between the CO<sub>2</sub> molecules and the active sites on the adsorbent surface, while the desorption profile reflects the thermal stability and binding energy of the adsorbed species. Thus, instead of a single material operating across all temperature regimes, materials tailored with varied binding site strengths are required to target low to high adsorption temperatures. Recent studies have shifted toward developing "smart sorbents" that can respond to temperature variations by adjusting their adsorption behaviour accordingly.

Manganese-based materials are widely recognized for their redox flexibility, thermal stability, and variable surface characteristics, making them excellent candidates for CO<sub>2</sub> capture.<sup>6</sup> The use of manganese oxides introduces moderate basic sites that are favourable for the chemisorp-

tion of acidic  $\mathrm{CO}_2$  molecules. However, the performance of Mn-based adsorbents alone may be limited by their surface area and pore accessibility. To improve their efficiency, especially under varying thermal conditions, the incorporation of a second metal has been widely explored in the literature.

The combination of manganese with a second metal oxide – such as potassium (K), calcium (Ca), or copper (Cu) – has been investigated to improve CO<sub>2</sub> capture performance. Wang et al.<sup>7</sup> had reported that potassium is well known for enhancing surface basicity, which facilitates CO<sub>2</sub> chemisorption. Study confirmed the calcium can form stable carbonates at elevated temperatures, contributing to long-term CO<sub>2</sub> retention and storage.<sup>8</sup> Meanwhile, copper provides redox-active sites and enhances moderate binding interactions through catalytic surface activation.<sup>9</sup> Bimetallic systems often display improved adsorption profiles, broader active site distributions, and stronger structural stability than their monometallic counterparts.

A new star in adsorbent support of fibrous silica KCC-1, is introduced to provide a playground for highly dispersed of active site and improved gas-solid interactions. Besides, it has large surface area, mesoporous architecture, and distinctive fibrous shape. For example, Nasir et al. investigated the performance of amine-functionalised KCC-1, where TEPA@KCC-1 exhibited a CO2 adsorption capacity of 4.31 mmol/g under 40 °C and 30 bar of maximum pressure. This study aims to open up new options for creating "temperature-smart" sorbents that can give targeted CO2 capture performance throughout low, medium, high and extremely high temperature ranges by co-loading manganese onto KCC-1 with K, Cu, or Ca.

An ultrasonic-surfactant-assisted impregnation technique was used to create the adsorbents, which ensured uniform dispersion, preventing from agglomerate and optimal interaction between the metals and the KCC-1 support. In addition to showcasing the exceptional adaptability of Mn-based bimetallic adsorbents, this work offers a guide for customizing materials to satisfy the ever-changing needs of sustainable CCS technology. This work clears the path for creative answers to one of the most important global issues of our day by connecting basic material science with real-world application.

### 2. Methodology

### 2. 1. Synthesis of Metals-Mn@KCC-1 Adsorbents

All chemicals used in this study were of analytical grade and applied without further purification. Tetraethyl orthosilicate (TEOS, Merck) was used as the silica precursor for the synthesis of KCC-1. Toluene (R&M Chemicals) served as the oil phase, while 1-butanol (Merck) acted as

the co-surfactant. Urea (Merck, Germany) was added to promote hydrolysis and condensation reactions. Cetyltrimethylammonium bromide (CTAB, Sigma-Aldrich) was used as the structure-directing agent during the synthesis of KCC-1 and also in the metal impregnation step. Distilled water was used in all solution preparations.

The fibrous silica KCC-1 support was synthesized using a microemulsion method as reported by Yusof et al. 13 with modifications involving ultrasonic and surfactant-assisted impregnation. In the metal loading step, approximately 1 g of KCC-1 was dispersed in 10 mL of distilled water and sonicated for 10 minutes. Metal precursors manganese(II) nitrate tetrahydrate Mn(NO<sub>3</sub>)<sub>2</sub>·4H<sub>2</sub>O (Sigma-Aldrich), potassium nitrate KNO<sub>3</sub> (R&M Chemicals), calcium nitrate tetrahydrate Ca(NO<sub>3</sub>)<sub>2</sub>·4H<sub>2</sub>O (Merck), and copper(II) nitrate trihydrate Cu(NO<sub>3</sub>)<sub>2</sub>·3H<sub>2</sub>O (Merck) were prepared separately in distilled water in a 1:1 molar ratio (Mn to co-metal) to achieve a 2.5 wt% loading for each metal. CTAB was added to the metal solution at a metal-to-surfactant ratio of 3:10 and sonicated for another 10 minutes.

The metal-containing solution was then mixed with the KCC-1 suspension and further sonicated for 30 minutes to ensure uniform distribution of metals on the support. The resulting mixture was dried on a hotplate at 80 °C until water completely evaporated. The adsorbents were thermally treated (calcined) at 600 °C for 4 hours under nitrogen to remove the residual CTAB surfactant and stabilize the metal oxides, this process is referred to as activation. The final adsorbents were designated as M-MnO@ KCC-1, where M refers to  $K_2O$ , CaO, or CuO depending on the co-metal used.

### 2. 2. Characterization

The structural, chemical, morphological, and textural properties of the prepared adsorbents were evaluated using several characterization techniques. X-ray diffraction (XRD) analysis was performed using a Bruker D8 Advance diffractometer with Cu-K $\alpha$  radiation ( $\lambda = 1.5406 \text{ Å}$ ), operated at 40 kV. The scans were recorded over a  $2\theta$  range of 10° to 80° with a step size of 0.02°. Fourier Transform Infrared (FTIR) spectra were obtained using an Agilent Cary 600 in the range of 4000–400 cm<sup>-1</sup> at a resolution of 4 cm<sup>-1</sup> with 32 scans per sample. Nitrogen adsorption-desorption isotherms were recorded at 77 K using a Micromeritics Tristar II Plus analyser after degassing the samples at 150 °C for 4 hours under flow of nitrogen gas. The BET method was used to determine surface area, while the Barrett-Joyner-Halenda (BJH) method was applied to derive the pore size distribution from the desorption branch. The surface morphology and elemental distribution were studied using field emission scanning electron microscopy (FESEM) and energy dispersive X-ray spectroscopy (EDX), both conducted on a Zeiss Merlin Compact operated at an accelerating voltage of 5-15 kV.

### 2. 3. CO<sub>2</sub> Capture Study

The CO<sub>2</sub> capture performance of the adsorbents was evaluated using temperature-programmed desorption of CO<sub>2</sub> (TPD-CO<sub>2</sub>). Prior to the desorption step, each sample (approximately 20 mg) was pretreated under a flow of high-purity nitrogen gas (99.999%) at 150 °C for 1 h to remove any physisorbed species. After cooling to 50 °C, the samples were exposed to a continuous flow of 15 % CO<sub>2</sub> balanced with nitrogen at a total flow rate of 15 mL/ min for 1 hour to allow adsorption. The adsorption was carried out under saturation mode to ensure complete CO<sub>2</sub> coverage on all available active sites. Following adsorption, the system was purged with nitrogen at the same flow rate for 30 minutes to remove any weakly physisorbed CO<sub>2</sub>. The desorption step was then carried out by heating the sample from 50 °C to 900 °C at a rate of 10 °C/min under a nitrogen flow of 15 mL/min. The CO<sub>2</sub> desorption profile was monitored using a thermal conductivity detector (TCD). The desorption patterns obtained were used to analyse the strength and distribution of the CO2 adsorption sites across the tested temperature range.

### 3. Result And Discussion

# 3. 1. Physicochemical Properties of Adsorbents

The structural and composition of Mn co-loaded with potassium (K), calcium (Ca), and copper (Cu) on the

fibrous silica KCC-1 support are revealed by the XRD patterns (Figure 1a). All samples exhibit a broad diffraction peak at 15–35°, which is consistent with the amorphous silica structure framework of the KCC-1. 14,15 The typical broad peak associated to the fibrous silica structure's preservation, which is necessary to sustain the large surface area and porosity required for CO<sub>2</sub> capture capacity and the metal dispersion. The absence of noticeable MnO peaks indicates that manganese oxide is well-distributed throughout the KCC-1 surfaces, with particle sizes due to falling below the XRD technique's detection limit.

None of the CaO peaks exist for CaO-MnO@KCC-1 due to the calcium and manganese substrates are widely distributed throughout the KCC-1 surface, making crystallinity invisible to XRD. The CuO-MnO@KCC-1 sample exhibited a peak at 34°, which corresponds to MnO (111) (ICDD 03-065-0638), indicating the existence of crystalline manganese oxide due to increased crystallinity and larger MnO particle domains, which exceed the XRD detection threshold. Strong interactions between copper and the silica framework were also suggested by the identification of a peak at 46° as copper silicate (431) (ICDD 03-032-0346), resulting imbedded of copper mostly on the dendrimer of KCC-1 (outer surface).

Significant peaks in the FTIR spectra of K<sub>2</sub>O-MnO@ KCC-1, CaO-MnO@KCC-1, and CuO-MnO@KCC-1 validate the chemical and structural properties of the produced materials. The asymmetric stretching and bending vibrations of the Si-O-Si framework are responsible for the strong and broad absorption bands seen in the 800-

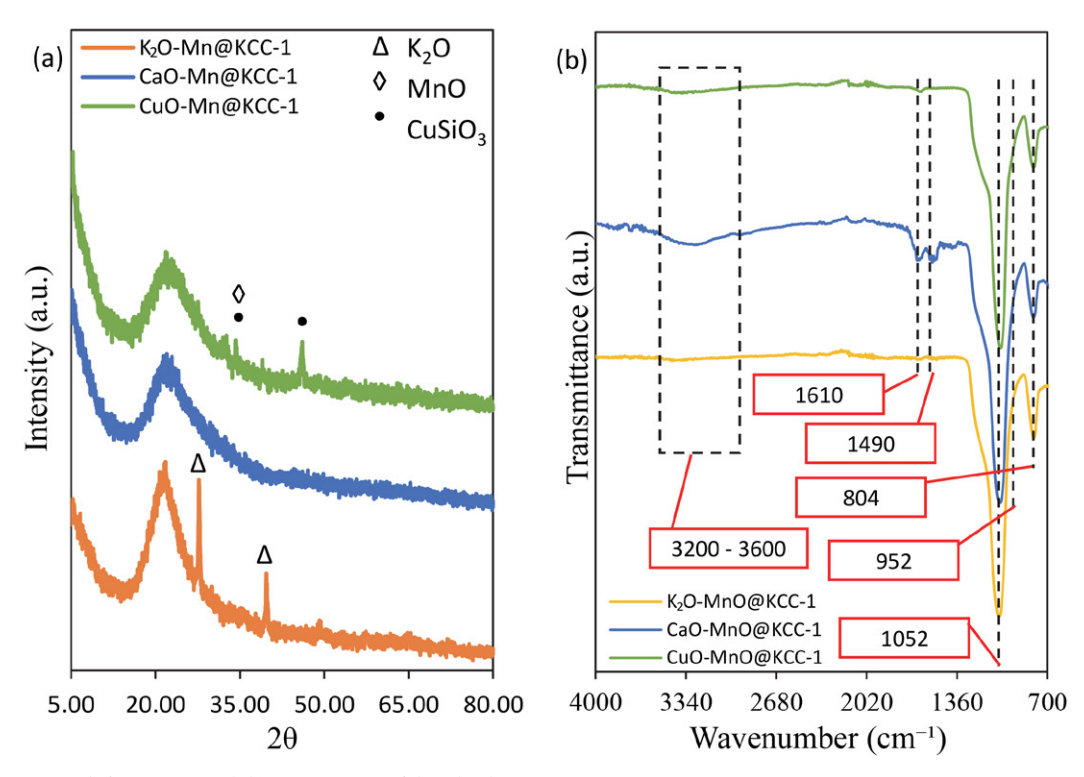


Figure 1: (a) XRD diffractogram and (b) FTIR spectra of the adsorbents.

850 cm<sup>-1</sup> and 1100–1200 cm<sup>-1</sup> ranges for all adsorbents. <sup>16,17</sup> These peaks validate the mesoporous properties of the silica structure by showing that it has been preserved inside the KCC-1 framework. All adsorbents exhibit a wide band in the high-frequency range at around 3400 cm<sup>-1</sup>, which is ascribed to the stretching vibrations of hydroxyl (–OH) groups. <sup>18,19</sup> The presence of surface hydroxyls, which are essential for adsorbent interactions, including the adsorption of molecules like CO<sub>2</sub>, is shown by this peak. Due to variations in surface chemistry brought about by the added metals (K, Ca, and Cu), the hydroxyl peak's strength may fluctuate somewhat between the samples due to the hygroscopic of metal particles properties.

The spectra show clear peaks for CaO-MnO@KCC-1 at 1610 cm<sup>-1</sup> and 1490 cm<sup>-1</sup>. The peak of H-O-H bending vibration is shown at 1610 cm<sup>-1</sup> indicates molecularly adsorbed water.<sup>20</sup> This is attributed to the strong basicity of CaO, which readily reacts with atmospheric CO<sub>2</sub>. The existence of calcium oxide species is suggested by the peak at 1490 cm<sup>-1</sup>, which is attributed to CaO.<sup>21</sup> These results are consistent with the XRD data, which demonstrate the well-dispersed nature of calcium species on the KCC-1 framework but do not reveal any identifiable CaCO<sub>3</sub> peaks. A carbonate peak also appears for CuO-MnO@KCC-1 at 1610 cm<sup>-1</sup>, which is consistent with the Cu silicate phases shown by XRD. The presence of carbonate indicates that copper and CO<sub>2</sub> may interact partially, possibly resulting in the formation of weakly bonded carbonates. The idea that copper species are evenly distributed or imbedded in the silica network is supported by the lack of noticeable CuO peaks in XRD. Copper preserves the mesoporous structure of silica while improving redox characteristics that are essential for mild CO2 adsorption, according to the FTIR data. When compared to XRD, the FTIR results highlight how each metal affects the structural and chemical characteristics of the KCC-1 support. Copper interacts with the silica framework to contribute to mild CO<sub>2</sub> adsorption, but calcium promotes a high basicity with persistent carbonate and oxide forms. The structural and functional changes by the metal impregnation in KCC-1 are better understood according to these combined findings analysis.

The textural properties of the synthesized adsorbents were investigated using nitrogen adsorption—desorption isotherms, pore size distribution (PSD), and BET surface area measurements. All samples exhibit Type IV isotherm with an H1 hysteresis loop, as shown in Figure 2, which is characteristic of mesoporous materials. The presence of

this loop indicates capillary condensation in mesopores and confirms that the mesoporous structure of KCC-1 was preserved after metal impregnation. The size of the hysteresis loop varied among the samples, with CuO-MnO@ KCC-1 showing a visibly wider loop compared to the other two, indicating a higher pore volume and more developed mesoporous structure as reported before by Maity and Polshettiwar.<sup>22</sup>

Table 1 presents the BET surface area, total pore volume, and average pore size of all samples. The  $K_2O\text{-MnO@}$  KCC-1 sample provide the lowest surface area (71 m²/g) and pore volume (0.17 cm³/g), with an average pore diameter of 9.6 nm. Compared to pristine KCC-1 reported by Hao et al.,²³ which has a BET surface area of approximately 600 m²/g, a pore volume of 0.91 cm³/g, and an average pore size of 7.1 nm, this indicates a significant reduction in textural properties, likely due to partial pore blockage by potassium oxide. This is further supported by the broader and less intense PSD peak of  $K_2O\text{-MnO@KCC-1}$  in Figure 3, suggesting reduced pore uniformity and lower accessibility, which is consistent with previous findings by Yusof et al.  $^{13}$ 

In contrast, CaO-MnO@KCC-1 exhibited a much higher surface area (296 m²/g) and pore volume (0.52 cm³/g), with an average pore diameter of 6.6 nm. The PSD shows a sharper and narrower peak compared to  $K_2O-MnO@KCC-1$ , indicating more uniform mesopores. The smaller average pore size observed here is not necessarily stabilizing the structure, but rather reflects the formation of more compact pore networks due to calcium oxide distribution within the KCC-1 matrix. The shift in PSD toward smaller pore diameters suggests a densification of the pore network by CaO incorporation, as reported by Khine et al.8 without inducing pore collapse.

CuO-MnO@KCC-1 demonstrated the most favourable textural features, with the highest surface area (427 m²/g), largest pore volume (0.86 cm³/g), and an average pore size of 7.7 nm. Its isotherm shows a large and well-defined hysteresis loop, wider than those of the other samples, which supports the presence of well-developed mesopores and enhanced gas accessibility. The PSD curve shows moderately uniform pores, suggesting that copper oxide is well integrated and enhances the pore structure without severe blockage. This behaviour is consistent with the formation of copper silicate phases at the dendritic outer layers of KCC-1, as also supported by FESEM and XRD findings. The comparison of PSD peaks clearly shows a shift: Pristine KCC-1: ~7.1 nm,²3 K₂O-MnO@KCC-1:

Table 1: Textural properties of the adsorbents

Samples	BET surface area (m <sup>2</sup> /g)	Micropore area (m <sup>2</sup> /g)	Total pore volume (cm <sup>3</sup> /g)	Average pore size (nm)
K <sub>2</sub> O-MnO@KCC-1	71	2.0	0.17	9.6
CaO-MnO@KCC-1	296	5.7	0.52	6.6
CuO-MnO@KCC-1	427	13.2	0.86	7.7

9.6 nm (broader, less defined), CaO-MnO@KCC-1: 6.6 nm (narrow, sharp peak) and CuO-MnO@KCC-1: 7.7 nm (moderately broad). These differences indicate that potassium caused pore expansion but reduced uniformity, calcium led to narrower and denser pore channels, and copper enhanced mesoporosity while maintaining good pore accessibility. Overall, the copper-containing sample exhibits

the best balance of surface area, pore volume, and mesostructural quality.

All of the adsorbents' FESEM images (Figure 4) show KCC-1's distinctive fibrous structure, demonstrating that the spherical, dendritic mesoporous silica framework was successfully synthesized.<sup>22</sup> When metal oxides are added, the fibrous and unique morphology further demonstrate

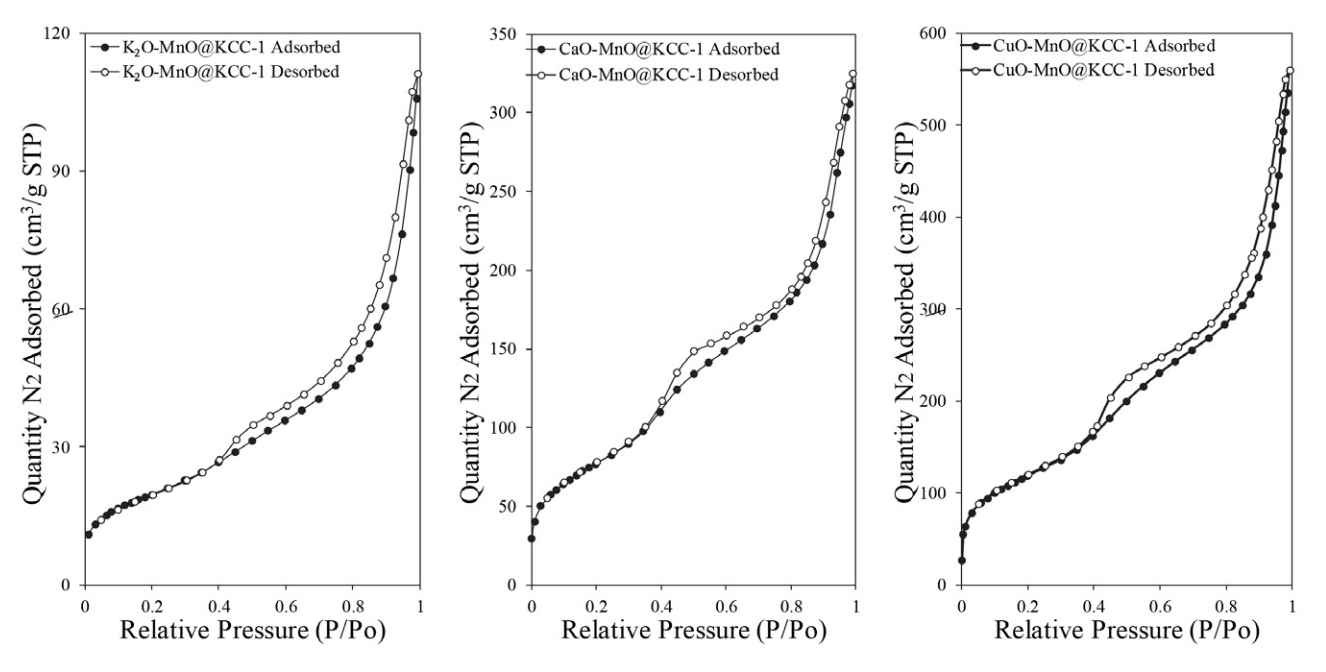


Figure 2: Nitrogen adsorption-desorption isotherm of adsorbents

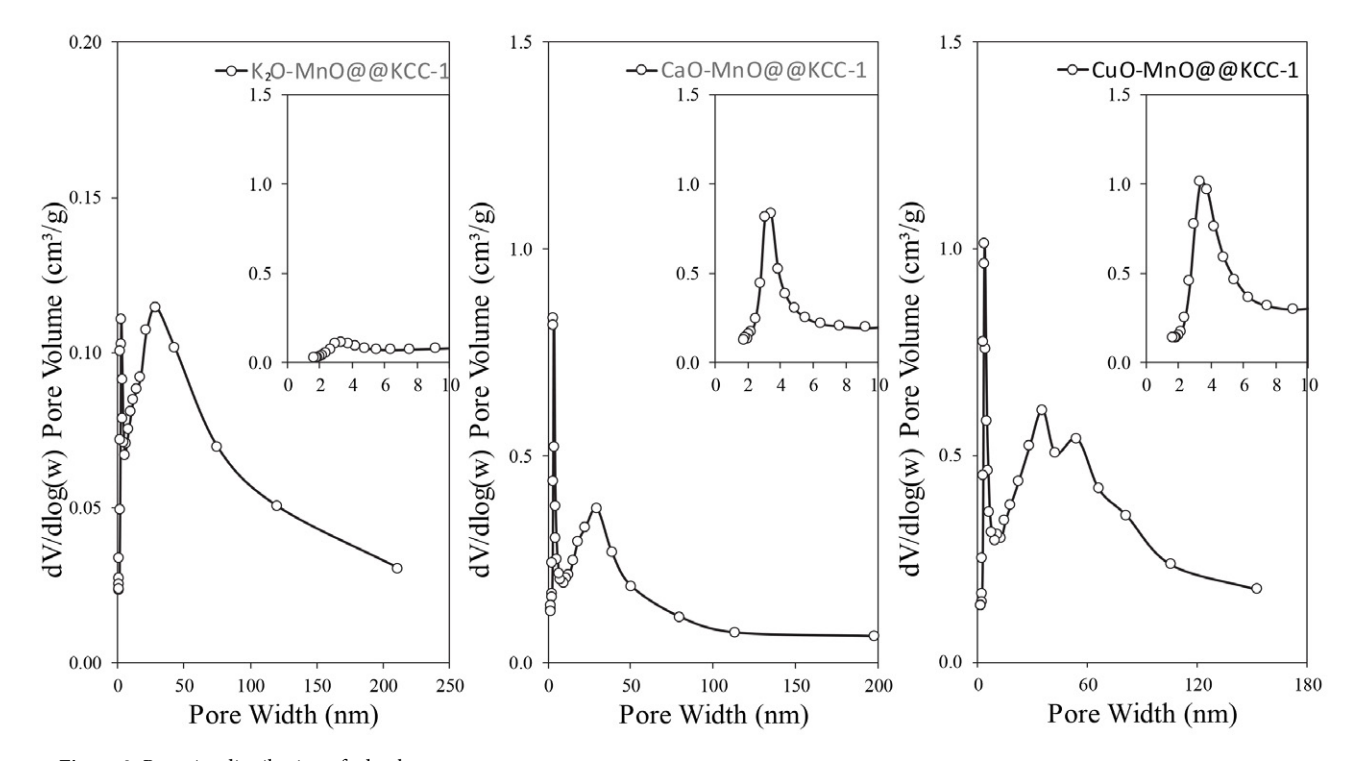


Figure 3: Pore size distribution of adsorbents

the KCC-1 framework's structural stability. However, K<sub>2</sub>O-MnO@KCC-1, CaO-MnO@KCC-1, and CuO-MnO@KCC-1 all have somewhat different particle morphologies and surface textures, which offer insight on how metal impregnation affects the adsorbents structure. The FESEM images of K<sub>2</sub>O-MnO@KCC-1 reveal that the fibrous network is mostly intact, but the surface seems somewhat rougher than that of pure KCC-1.<sup>24</sup>

Comparing CaO-MnO@KCC-1 to K<sub>2</sub>O-MnO@ KCC-1, the FESEM pictures reveal more distinct fibrous structure and extremely homogeneous spherical particles. The mesoporous structure's stability and integrity are reflected in this morphology, which is in line with the nitrogen adsorption data's narrow pore size distribution and larger BET surface area. The FTIR spectra ascribed to CaO and CaCO<sub>3</sub>, indicate that the structural framework is strengthened by calcium incorporation. These results are in line with the XRD data, which show that calcium has a synergistic impact on maintaining the mesoporous architecture by confirming well-dispersed calcium species without noticeable pore collapse. In con-

trast to CaO-MnO@KCC-1, CuO-MnO@KCC-1 exhibits a somewhat finer surface and well-preserved spherical shape, according to the FESEM images. The large BET surface area and the somewhat uniform pore size distribution, which is centred at 7.73 nm, are consistent with this finding. The presence of carbonate peaks in the FTIR spectrum indicates that there are not many interactions between the silica framework and copper species. The XRD data, which show evenly distributed copper species devoid of notable crystalline CuO peaks, support the FE-SEM findings that copper impregnation slightly decrease porosity without seriously harming the KCC-1 framework's structural integrity.

Important information on the elemental makeup of the adsorbents K<sub>2</sub>O-MnO@KCC-1, CaO-MnO@KCC-1, and CuO-MnO@KCC-1 and their effective integration into the silica framework is provided by the Energy-Dispersive X-ray (EDX) study (Figure 4). The existence of silicon (Si) and oxygen (O), the main constituents of the KCC-1 silica matrix, as well as manganese (Mn) and the corresponding metal modifiers potassium (K), calcium (Ca),

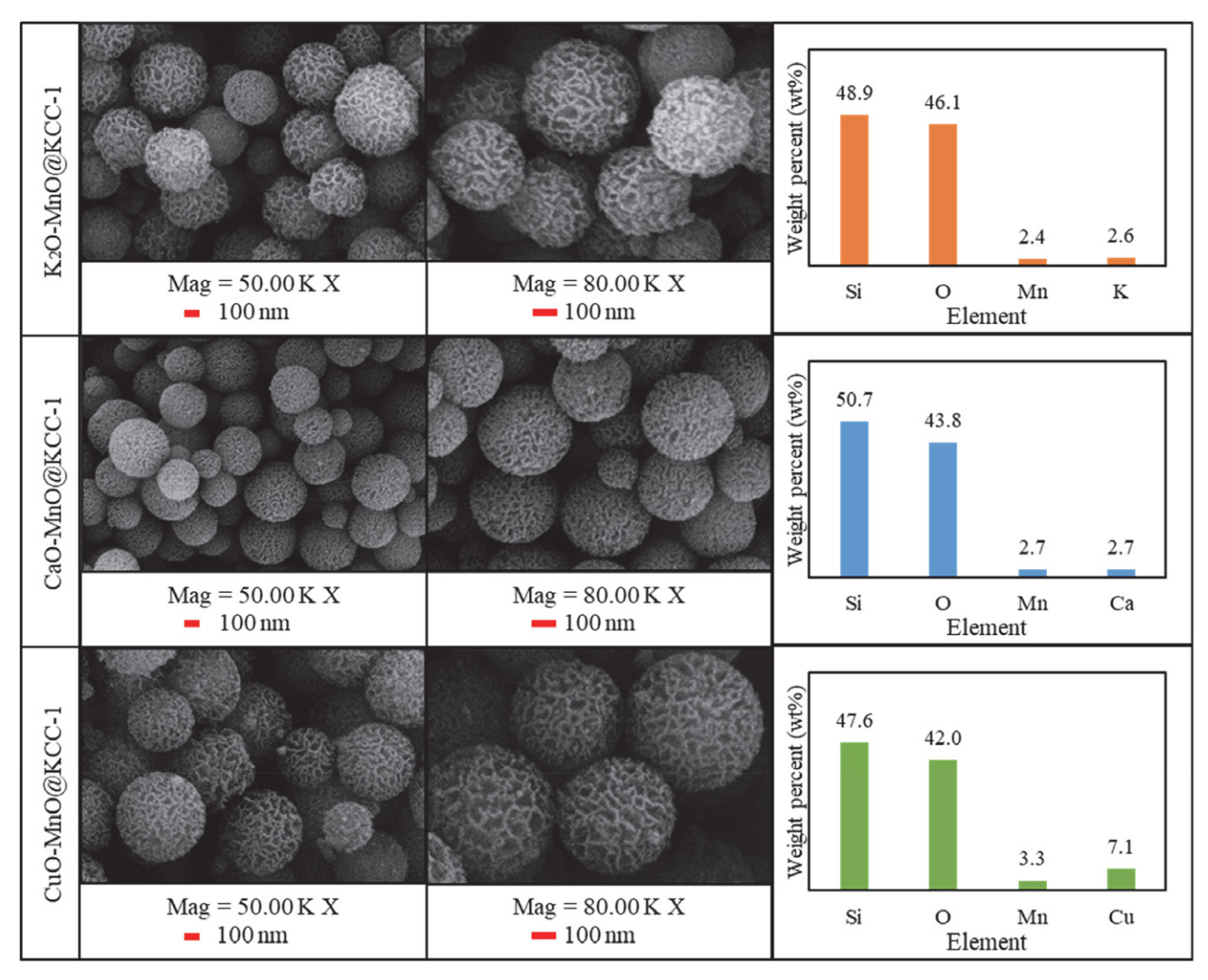


Figure 4: FESEM images and EDX of the adsorbents

and copper (Cu) are confirmed by the EDX spectra of all three materials. In conclusion, the FESEM and EDX study offers an understanding of the structural changes of metal impregnation when combined with XRD, FTIR and  $N_2$  adsorption-desorption data. CaO-MnO@KCC-1 exhibits improved stability and porosity because to calcium stabilizing impact, whereas  $K_2$ O-MnO@KCC-1 displays partial structural disruption. Conversely, CuO-MnO@KCC-1 preserves a balance between high porosity and structural integrity, which is a result of copper efficient interaction with the silica framework. These differences demonstrate how important the added metals in modifying the KCC-1-based adsorbents structural and textural characteristics.

### 3. 2. CO<sub>2</sub> Capture Study

Different CO<sub>2</sub> desorption peaks that correspond to weakly (<250 °C), moderately (251-480 °C), strong (481-700 °C) and very strong (>700 °C) adsorbed CO<sub>2</sub> species are shown in Figure 5 with tabulate in Table 2 (TPD-CO<sub>2</sub> profiles of each adsorbent).<sup>26</sup> The peaks for K<sub>2</sub>O-MnO@ KCC-1 are mostly weakly bound CO2 species, suggesting low adsorption energy locations where potassium oxide predominates and the adsorption at 14.74 cm<sup>3</sup>/g compared to pristine KCC-1 at 11.65 cm<sup>3</sup>/g reported by Yusof et al.<sup>12</sup> Although potassium increases basicity and improves interaction with acidic CO2 molecules, active sites are less accessible due to partial pore blockage. As a result, especially at higher temperatures, the adsorption capability is increase slightly. Because of potassium prevailing effect, manganese in K<sub>2</sub>O-MnO@KCC-1 appears to improve mild CO<sub>2</sub> binding but does not considerably enhance adsorption. On the other hand, very strong, moderate, and weak desorption peaks demonstrate the better adsorption capability of CaO-MnO@KCC-1 at 22.35 cm<sup>3</sup>/g. CaO plays a major role in the basicity of the material, which results in strong interactions with CO<sub>2</sub> and the development of carbonates on the surface. The desorption of tightly bonded CO<sub>2</sub> species is shown by the steep peak at higher temperatures, which suggests persistent carbonate production. Manganese function in this system is to balance the adsorption energies by offering sites for moderate CO<sub>2</sub> binding, which enhances the strong basic sites that calcium introduces. Among the three adsorbents, CaO-MnO@KCC-1 is the most effective due to its high affinity and dispersion, 8,25 which further improve the accessibility of active sites.

The TPD-CO<sub>2</sub> profile for CuO-MnO@KCC-1 displays a wider range of desorption peaks, covering weak, moderate, and high binding energies at 19.12 cm<sup>3</sup>/g. Manganese promotes CO<sub>2</sub> interaction at higher binding energies, whereas copper's redox characteristics improve moderate CO<sub>2</sub> adsorption through surface activation. The high adsorption peak is less noticeable than in CaO-MnO@ KCC-1, however, suggesting that there are fewer stable carbonate-forming sites. Given its high surface area and moderate pore size distribution, which enable quick CO<sub>2</sub> capture and release, it appears that CuO-MnO@KCC-1 depends more on dynamic adsorption-desorption processes than on strong chemical binding.27 When comparing the adsorbents, manganese presence in all systems is crucial for improving moderate adsorption sites and bridging the gap between the co-loaded metals capacities. Manganese partially mitigates the poor adsorption of potassium in K<sub>2</sub>O-MnO@KCC-1, whereas it enhances the strong binding of calcium in CaO-MnO@KCC-1, resulting in a wider variety of adsorption sites. For CuO-MnO@ KCC-1, manganese strengthens the material ability to bind CO<sub>2</sub> moderately and ensures stable performance across varying conditions. To sum up, the TPD-CO<sub>2</sub> data demonstrate how manganese and the co-loaded metals interact to influence adsorption efficiency. Copper encourages moderate adsorption, calcium strengthens strong carbonate production, while potassium favours weak binding. All the adsorbents demonstrate a beneficial synergistic interaction with manganese, contributing to a balanced distribution of CO2 adsorption sites across weak, moderate, and strong binding regions. As illustrated in Figure 5, CaO-MnO@KCC-1 exhibits the most comprehensive and intense desorption profile, indicating a high density of active basic sites. Its significant CO<sub>2</sub> uptake over a broad temperature range confirms its superior adsorption performance. This can be attributed to the presence of strong basicity, thermally stable carbonate formation, and a well-preserved mesoporous structure, making CaO-MnO@KCC-1 the most promising candidate for efficient CO<sub>2</sub> capture under varying operational conditions.

### 4. Conclusion

In order to improving their CO<sub>2</sub> adsorption capabilities, manganese was co-loaded onto dendritic fibre silica

Table 2: CO<sub>2</sub> Adsorption capacity of the adsorbents

Samples	CO <sub>2</sub> adsorption capacity (cm <sup>3</sup> /g)					
	Weak (<250 °C)	Medium (251–480 °C)	Strong (481–700 °C)	Very Strong (>700 °C)	Total	
K <sub>2</sub> O-MnO@KCC-1	3.38	9.89	_	1.48	14.74	
CaO-MnO@KCC-1	6.13	7.46	_	8.72	22.35	
CuO-MnO@KCC-1	3.23	8.91	_	6.98	19.12	

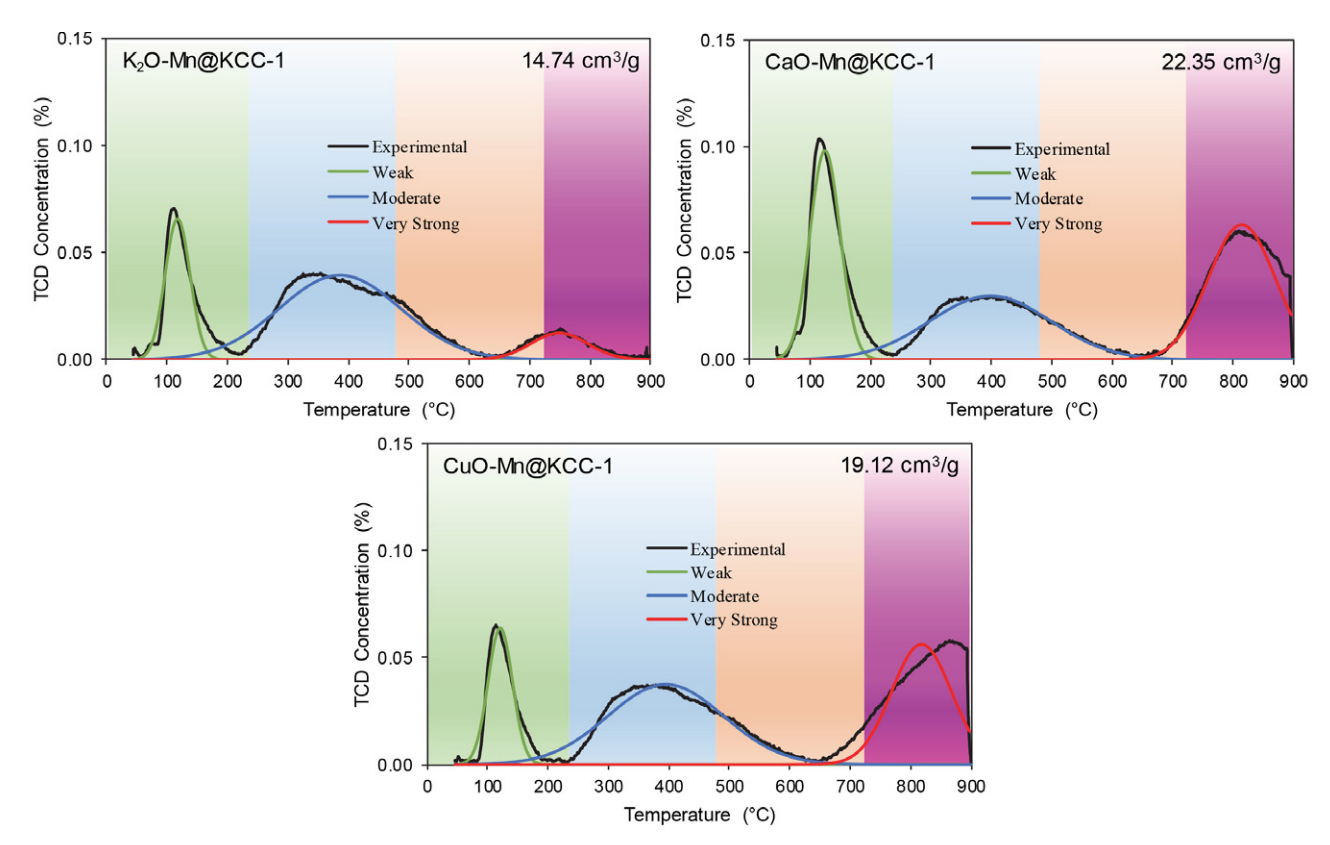


Figure 5: TPD-CO $_2$  profile of the adsorbents.

KCC-1 together with potassium, calcium, and copper. The characterization results demonstrated that metals were successfully incorporated into the KCC-1 framework, with distinct effects of each metal on the chemical, structural, and textural characteristics. According to TPD-CO<sub>2</sub> analysis, K<sub>2</sub>O-MnO@KCC-1 mainly prefers weakly bound CO<sub>2</sub> species, CaO-MnO@KCC-1 has a higher adsorption capacity because of its strong basicity and stable carbonate formation, and CuO-MnO@KCC-1 has redox characteristics allow it to efficiently balance moderate and strong adsorption sites. The results illustrate how manganese plays a crucial role in enhancing each metals adsorption behaviour. CaO-MnO@KCC-1 was found to be the most efficient adsorbent, indicating its potential for tailored CO<sub>2</sub> capture throughout a range of temperatures.

### AKNOWLEDGEMENT

The authors would like to acknowledge the funding support provided by Universiti Putra Malaysia under grant number 9795800 and the authors also express their gratitude to OCIM Sdn. Bhd. for supporting this research through grant number 6300940 awarded to Universiti Putra Malaysia.

### **Author contributions**

S.M.Y. and A.H.L. designed and performed the experiments. S.M.Y., S.S.S., S.S., and A.H.A.Z. performed the studies and data analysis. A.H.L, N.A.M. and U.K.N. su-

pervised the research. All authors contributed to the writing and editing of the manuscript.

### **Conflicts of interest**

The authors declare no conflicts of interest.

### 5. References

- S. A. Rawool, Y. Kar, V. Polshettiwar, *Mater. Adv.* 2022, 3, 8449–8459. DOI:10.1039/D2MA00809B
- Y. Guo, L. Luo, Y. Zheng, T. Zhu, ACS Omega 2020, 5, 9641–9648. DOI:10.1021/acsomega.9b03374
- M. Younas, M. Sohail, L. L. Kong, M. J. K. Bashir, S. Sethupathi, *Int. J. Environ. Sci. Technol.* 2016, 13, 1839–1860.
   DOI:10.1007/s13762-016-1008-1
- S. Y. Lee, S. J. Park, J. Ind. Eng. Chem. 2015, 23, 1–11.
   DOI:10.1016/j.jiec.2014.09.001
- N. Mittal, A. Samanta, P. Sarkar, R. Gupta, *Energy Sci. Eng.* 2015, 3, 207–220. DOI:10.1002/ese3.64
- V. Mahdavi, M. Mardani, *Mater. Chem. Phys.* 2015, 155, 136–146. DOI:10.1016/j.matchemphys.2015.02.011
- S. Wang, J. Zhan, K. Chen, A. Ali, L. Zeng, H. Zhao, W. Hu, L. Zhu, X. Xu, ACS Sustain. Chem. Eng. 2020, 8, 8214–8222.
   DOI:10.1021/acssuschemeng.0c01151
- E. E. Khine, D. Koncz-Horvath, F. Kristaly, T. Ferenczi, G. Karacs, P. Baumli, G. Kaptay, *J. Nano. Res.* 2022, 24, 139.
   DOI:10.1007/s11051-022-05518-z

- B. Boukoussa, A. Hakiki, N. Bouazizi, A. P. Beltrao-Nunes, F. Launay, A. Pailleret, F. Pillier, A. Bengueddach, R. Hamacha, A. Azzouz, *J. Mol. Struct.* 2019, 1191, 175–182.
   DOI:10.1016/j.molstruc.2019.04.035
- K. Palanichamy, S. Umasankar, S. Ganesh, N. Sasirekha, *Int. J. Hydrogen Energy* **2023**, 48, 11727–11745.
   **DOI:**10.1016/j.ijhydene.2022.12.076
- M. S. R. M. Nasir, M. P. Khairunnisa, N. W. C. Jusoh, A. A. Jalil, *IOP Conf. Ser. Earth Envi. Sci.* 2020, 476, 1, 12084.
   DOI:10.1088/1755-1315/476/1/012084
- H. Hamrayev, S. Korpayev, K. Shameli, J. Res. Nanosci. Nanotechnol. 2024, 12, 1–24. DOI:10.37934/jrnn.12.1.124
- 13. S. M. Yusof, R. Othaman, H. D. Setiabudi, L. P. Teh, *J. Solid State Chem.* **2021**, *294*. **DOI:**10.1016/j.jssc.2020.121845
- S. N. Bukhari, C. C. Chong, H. D. Setiabudi, Y. W. Cheng, L. P. Teh, A. A. Jalil, *Chem. Eng. Sci.* 2021, 229, 116141.
   DOI:10.1016/j.ces.2020.116141
- M. S. R. M. Nasir, M. P. Khairunnisa, N. W. C. Jusoh, A. A. Jalil, *IOP Conf. Ser. Mater. Sci. Eng.* 2020, 808, 012031.
   DOI:10.1088/1757-899X/808/1/012031
- M. Safar, B. J. Lin, W. H. Chen, D. Langauer, J. S. Chang, H. Raclavska, A. Pétrissans, P. Rousset, M. Pétrissans, *Appl. Energy* 2019, 235, 346–355. DOI:10.1016/j.apenergy.2018.10.065
- Q. Li, H. Zhang, F. Peng, C. Wang, H. Li, L. Xiong, H. Guo, X. Chen, *Energ. Fuel.* 2020, 4, 2097–2106.
   DOI:10.1021/acs.energyfuels.9b03997

- M. Pishnamazi, H. Hafizi, M. Pishnamazi, A. Marjani, S. Shirazian, G. M. Walker, *Sci. Rep.* 2021, *11*, 535.
   DOI:10.1038/s41598-020-79983-8
- X. Yan, X. Hu, S. Komarneni, RSC Adv. 2014, 4, 57501–57504.
   DOI:10.1039/C4RA09626F
- F. Zarei, A. Marjani, A. Hassani Joshaghani, *J. Environ. Chem. Eng.* 2019, 7. DOI:10.1016/j.jece.2019.103309
- C. Diningsih, L. Rohmawati, *Indonesian Phys. Rev.* 2022, 5, 208–215. DOI:10.29303/ipr.v5i3.174
- W. Guan, F. Ji, Y. Cheng, Z. Fang, D. Fang, P. Yan, Q. Chen, J. Nanomater. 2013, 2013, 542109. DOI:10.1155/2013/542109
- 23. A. Maity, V. Polshettiwar, *Chem. Sus. Chem.* **2017**, *10*, 3866–3913. **DOI**:10.1002/cssc.201701076
- 24. P. Hao, B. Peng, B.Q. Shan, T.Q. Yang, K. Zhang, *Nanoscale Adv.* **2020**, *2*, 1792–1810. **DOI:**10.1039/D0NA00219D
- A. Maity, A. Das, D. Sen, S. Mazumder, V. Polshettiwar, *Langmuir* 2017, 33, 13774–13782.
- DOI:10.1021/acs.langmuir.7b02996
  26. A. H. Lahuri, M. A. Yarmo, T. S. Marliza, M. N. Abu Tahari, W. Z. Samad, N. Dzakaria, M. R. Yusop, *Mater. Sci. Forum.*
  - 2017, pp. 479–484.
  - DOI:10.4028/www.scientific.net/MSF.888.479
- W. N. R.W. Isahak, Z. A. C. Ramli, M. W. Ismail, K. Ismail, R. M. Yusop, M. W. M. Hisham, M. A. Yarmo, *J. CO<sub>2</sub> Util.* **2013**, 2, 8–15. **DOI**:10.1016/j.jcou.2013.06.002

### **Povzetek**

Nenehno naraščanje ravni CO<sub>2</sub> v ozračju zaradi industrijskih emisij in izgorevanja fosilnih goriv je povečalo potrebo po učinkovitem zajemanju ogljika. Trdni adsorbenti so priljubljeni zaradi možnosti večkratne uporabe in nizke porabe energije, vendar pogosto naletijo na omejitve v toplotni stabilnosti in adsorpcijski zmogljivosti. Ta študija preučuje učinek sočasnega nalaganja mangana (Mn) s kalijem (K), bakrom (Cu) in kalcijem (Ca) na vlaknasto siliko KCC-1 za zajemanje CO<sub>2</sub> v širokem temperaturnem območju. KCC-1 je bil sintetiziran z metodo mikroemulzije, kovine pa so bile dodane z ultrazvočno impregnacijo s pomočjo površinsko aktivnih snovi. Karakterizacija z uporabo XRD, FTIR, BET, FESEM-EDX in CO<sub>2</sub>-TPD je potrdila strukturno celovitost, funkcionalnost površine in adsorpcijsko obnašanje. CaO-MnO@KCC-1 kaže najbolj uravnotežene teksturne lastnosti in najvišjo absorpcijo CO<sub>2</sub> zaradi svoje močne bazičnosti in raznolike moči adsorpcijskih mest. To poudarja njegov potencial kot temperaturno prilagodljiv adsorbent CO<sub>2</sub>.



Except when otherwise noted, articles in this journal are published under the terms and conditions of the Creative Commons Attribution 4.0 International License